

Mitigating Long-Tail Bias in HOI Detection via Adaptive Diversity Caches

Yuqiu Jiang, Xiaozhen Qiao, Yifan Chen, Ye Zheng, Zhe Sun, and Xuelong Li, *Fellow, IEEE*

Abstract—Human-Object Interaction (HOI) detection is a fundamental task in computer vision, empowering machines to comprehend human-object relationships in diverse real-world scenarios. Recent advances in VLMs have significantly improved HOI detection by leveraging rich cross-modal representations. However, most existing VLM-based approaches rely heavily on additional training or prompt tuning, resulting in substantial computational overhead and limited scalability, particularly in long-tailed scenarios where rare interactions are severely under-represented. In this paper, we propose the Adaptive Diversity Cache (ADC) module, a novel training-free and plug-and-play mechanism designed to mitigate long-tail bias in HOI detection. ADC constructs class-specific caches that accumulate high-confidence and diverse feature representations during inference. The method incorporates adaptive capacity allocation favoring rare categories and dynamic feature augmentation to enable robust prediction calibration without requiring additional training or fine-tuning. Extensive experiments on HICO-DET and V-COCO datasets show that ADC consistently improves existing HOI detectors, particularly enhancing rare category detection while preserving overall performance. These findings confirm the effectiveness of ADC as a training-free, plug-and-play solution for long-tail bias mitigation.

Index Terms—HOI detection, VLMs, Test time adaptation.

I. INTRODUCTION

HUMAN-OBJECT Interaction (HOI) detection [1] stands as a cornerstone in computer vision, with broad applications in autonomous driving and robotic manipulation [2]–[10]. By identifying interactions between humans and objects, such as “holding a bottle” or “riding a bicycle”, HOI detection delivers enriched semantic understanding to facilitate advanced decision-making. Moreover, HOI detection serves as a foundational component for tasks like action recognition [11]–[15] and visual question answering [16]–[20].

Vision-Language Models (VLMs), such as CLIP [21] and Flamingo [22], achieve robust alignment between visual and language modalities through pre-training on large-scale image-text pairs. These models excel in zero-shot and few-shot learning tasks, effectively bridging the gap between visual features and semantic descriptions to provide rich cross-modal representations for downstream applications. As il-

Manuscript received Month Day, Year; revised Month Day, Year. (Corresponding author: Zhe Sun, Xuelong Li.)

Yuqiu Jiang is with the College of Future Information Technology, Fudan University, Shanghai, 200438, China. This work was done during a research internship at the Institute of Artificial Intelligence (TeleAI), China Telecom (E-mail: jyqiu03@gmail.com).

Xiaozhen Qiao is with the School of Information Science and Technology, University of Science and Technology of China, Hefei, 230026, China, and also with the Institute of Artificial Intelligence (TeleAI), China Telecom.

Yifan Chen, Ye Zheng, Zhe Sun and Xuelong Li are with the Institute of Artificial Intelligence (TeleAI), China Telecom (Corresponding author: sunzhe@nwpu.edu.cn, xuelong_li@ieee.org).

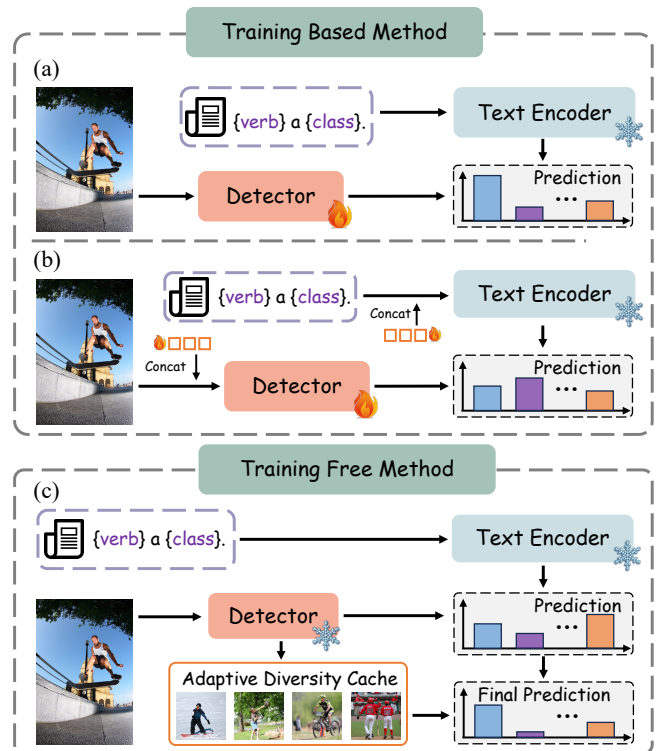


Fig. 1. Comparison of three HOI detection approaches. (a) Alignment-based model; (b) Prompt tuning-based model; (c) Our proposed training-free model.

lustrated in Fig. 1(a) and (b), existing VLM-based HOI detection approaches can be broadly categorized into two paradigms: alignment-based methods and prompt-based methods. Alignment-based methods integrate HOI-related visual features with pre-trained VLMs through feature alignment to exploit implicit knowledge for interaction recognition. These approaches typically employ knowledge distillation or feature optimization techniques to improve the alignment between visual and textual representations. In contrast, prompt-based methods adapt VLMs to HOI tasks via prompt learning without requiring major architectural modifications. Such methods introduce trainable prompts for multi-modal optimization and leverage guided prompt learning strategies to enhance model performance.

Despite the remarkable progress achieved in HOI recognition, existing methods remain reliant on additional training procedures. This reliance not only incurs substantial computational costs and the demand for large-scale annotated data, but also limits the scalability and deployment of HOI systems in real-world scenarios where annotation resources are scarce

or unavailable. Additionally, these training-based approaches often struggle to generalize to rare interactions, particularly under the long-tailed distribution prevalent in HOI datasets (see Fig. 2). A handful of frequent interactions dominate in such distributions, while rare HOIs are severely underrepresented. This imbalance induces significant prediction bias: models overfit to common categories during training, resulting in insufficient representations that inadequately capture the distinctive features of rare categories. It is important to note that the long-tail issue in HOI detection is multi-factorial. It stems not only from the frequency imbalance of object or verb categories but fundamentally from the *compositional sparsity* of HOI triplets [23]. Many valid human-object combinations appear rarely or never in the training set, making it difficult for models to learn robust visual prototypes for these “tail” compositions. Consequently, recognition performance on rare interactions deteriorates, severely limiting generalization to open-world scenarios.

To this end, this paper proposes the Adaptive Diversity Cache (ADC) module, a novel training-free and plug-and-play mechanism that can be integrated into existing HOI detectors, as illustrated in Fig. 1(c). ADC enables dynamic accumulation of high-confidence and diverse feature representations during inference, thereby enhancing the detection of rare interaction categories without requiring additional training or model modifications. The ADC module operates through two key mechanisms to address long-tail bias in HOI detection. First, it maintains a real-time, class-specific cache that selectively accumulates high-confidence and diverse features based on a joint confidence-diversity criterion. Second, ADC adaptively allocates cache capacity according to class frequency, assigning larger caches to rare categories to ensure effective representation, then it performs feature augmentation during inference by integrating real-time augmented features, which are then utilized in an affinity-based retrieval process to refine model predictions. Collectively, these mechanisms enable ADC to achieve efficient, training-free calibration at test time, improving the detection of rare interactions under long-tailed distributions while maintaining competitive performance on frequent categories. It is worth noting that the effectiveness of ADC extends beyond conventional supervised settings. For models specifically designed for zero-shot HOI detection (*e.g.*, EZ-HOI), ADC can amplify their inherent advantages by accumulating reliable interaction patterns in the cache. This characteristic makes ADC particularly valuable for enhancing zero-shot capable models.

The contributions of this paper can be summarized as follows:

- We propose the ADC module, a novel training-free and plug-and-play mechanism with broad applicability that effectively mitigates prediction bias under long-tailed distributions by leveraging a dynamic and adaptive feature caching mechanism during inference.
- We introduce two key components within ADC: confidence-diversity joint cache selection and frequency-aware cache adaptation, which collaboratively enhance rare interaction detection by balancing representational diversity and frequency-aware cache capacity, without

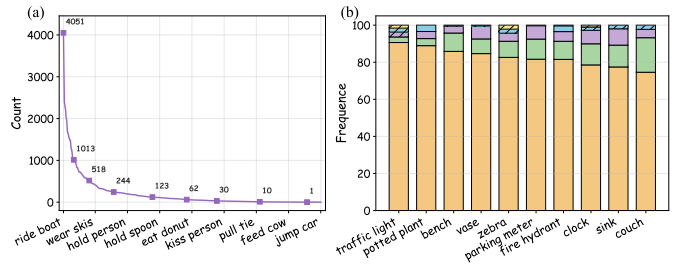


Fig. 2. Long-tail distribution of the HICO-DET dataset. (a) Distribution of HOI interaction frequencies shows extreme imbalance across different verb-object pairs, with the most frequent interaction having over 4000 instances, while many rare interactions have fewer than 10 instances. (b) Verb distribution for different objects demonstrates a severe imbalance, where dominant verbs account for over 90% of interactions for certain objects.

requiring any model retraining.

- Extensive experiments on multiple HOI benchmarks demonstrate that ADC consistently improves existing HOI detectors, achieving substantial performance gains on rare categories while preserving strong overall detection performance across different baseline architectures.

II. RELATED WORKS

A. Human-Object Interaction Detection

HOI detection aims to recognize interactions between humans and objects in visual scenes, addressing challenges in tasks like scene understanding and action recognition. HOI methods based on VLMs fall into two paradigms: alignment-based and prompt-based approaches. Alignment-based methods [24]–[27] align HOI visual features with pre-trained VLMs [28]–[30] to leverage their knowledge for interaction detection. Representative works include GEN-VLKT [24], which transfers CLIP [21] semantic representations through knowledge distillation, and HOICLIP [25], which directly utilizes VLM visual encoders for HOI feature extraction. Prompt-based approaches modify VLMs through prompt learning for HOI tasks [8], [9], [31]. Notable examples are MaPLe [31], which employs multi-modal prompt tuning, and EZ-HOI [9], which introduces guided prompt learning with foundation model guidance to enhance performance. However, these methods often require additional training or fine-tuning phases, rely on domain-specific designs, and are susceptible to noise in continuous data streams, leading to slow adaptation convergence.

B. Test Time Adaptation

Test-time adaptation (TTA) [32]–[34] aims to update a trained model on a single unlabeled test sample before making predictions to increase its robustness to distribution shift. Early TTA work primarily focused on image classification, with methods like TENT [33] minimizing entropy of model predictions, and others exploring self-supervised auxiliary tasks [35] and contrastive learning approaches [36]. Recent advances include TDA [37], which introduces a training-free dynamic adapter with key-value cache for efficient adaptation, and DPE [38], which evolves dual prototypes to accumulate

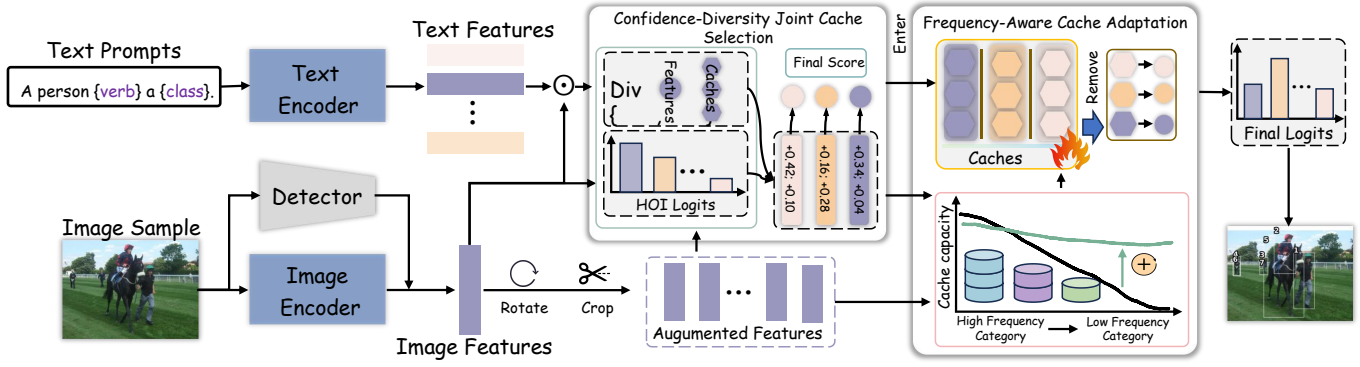


Fig. 3. Architecture Overview. Given an image and text prompts, region features are extracted via the image encoder and text features via the text encoder, yielding f_{vis} and f_{xt} . Interaction logits $\Phi = f_{\text{vis}} \cdot f_{\text{xt}}$ are computed and input to the Adaptive Diversity Cache module. ADC leverages confidence-diversity joint cache construction, adaptive capacity allocation, and dynamic cache augmentation to update feature caches and enhance rare class prediction dynamically. The final HOI logits $\text{logit}_{\text{final}}$ are obtained by fusing base and cache-augmented predictions.

task-specific knowledge from multi-modalities in VLMs. The success in classification has inspired applications to semantic segmentation [39], [40], image super-resolution [41], [42], and object detection [43], [44]. However, HOI detection [9], [25] presents unique challenges due to its compositional nature, where the same action can involve different objects and vice versa, making it particularly susceptible to domain shifts. Introducing TTA to HOI detection faces challenges, including complex pseudo-label generation for multi-faceted predictions, difficult confidence estimation for spatial-semantic relationships, and adaptation to long-tail HOI distributions. Despite these challenges, we present a novel plug-and-play module for test-time adaptation in HOI detection, aiming to address the long-tail problem and enable robust performance across diverse interaction patterns.

III. METHOD

This section introduces the Adaptive Diversity Cache (ADC) mechanism, a novel training-free and plug-and-play module designed to mitigate the long-tail bias in HOI detection. Unlike existing TTA methods (e.g., BoostAdapter [45]) that focus on parameter adaptation or feature distribution alignment for single-label classification, our ADC module addresses the compositional nature of HOI detection. While TDA employs key-value caches for feature adaptation, it lacks mechanisms to handle the severe class imbalance (long-tailed distribution) and compositional complexity inherent in HOI tasks.

The long-tailed distribution of HOI categories induces prediction bias in pre-trained models, characterized by reduced sensitivity to rare interaction classes. Let $\mathcal{D}_{\text{train}} = \{(x_i, y_i)\}$ denote the training set where $y_i \in \mathcal{Y}$ follows an imbalanced distribution $P_{\text{train}}(y)$, and $\mathcal{Y}_{\text{rare}} \subset \mathcal{Y}$ represents rare classes with limited training samples. This bias is formalized as:

$$\mathbb{E}_{y \sim P_{\text{test}}}[\mathbb{I}(f(x) = y)] \ll \mathbb{E}_{y \sim P_{\text{train}}}[\mathbb{I}(f(x) = y)] \quad (1)$$

$$\forall y \in \mathcal{Y}_{\text{rare}},$$

where $f(\cdot)$ denotes the HOI detector, and $\mathbb{I}(\cdot)$ is the indicator function. To address this, we propose the ADC module, which encompasses two core mechanisms: Confidence-

Diversity Joint Cache Selection, and Frequency-Aware Cache Adaptation.

A. Confidence-Diversity Joint Cache Selection

Inspired by Boostadapter [45], we posit that maintaining a historical prediction queue of HOI pair visual features alleviates inference bias from imbalanced data. This dynamic repository enables reference to diverse historical information, counteracting skewed learning from uneven class distribution.

To construct an effective cache capturing both high-confidence and diverse representations for each HOI pair, we propose *Confidence-Diversity Joint Cache Selection (CJCS)*, which jointly optimizes prediction confidence and feature diversity to retain representative samples while avoiding redundant information accumulation.

For each interaction class c , we maintain a priority queue $\mathcal{Q}_c = \{(f_k, h_k)\}_{k=1}^K$. Here, c denotes a tuple of object and verb (o, v) , f_k denotes visual features, and h_k represents prediction logits. The queue capacity is bounded by the shot capacity K , with initial queues empty ($\mathcal{Q}_c = \emptyset$).

To balance diversity and relevance to test samples, we introduce an adaptive selection criterion combining confidence and feature diversity. For a test sample x_t , we first predict its pseudo-label ℓ_t :

$$\ell_t = \arg \max_{y_c} \mathcal{D}(y = y_c | x_t), \quad (2)$$

where $\mathcal{D}(\cdot | x_t)$ denotes the model's prediction distribution over HOI classes. We then construct a temporary cache by incorporating x_t into the existing queue for class ℓ_t : $\mathcal{Q}_{\ell_t}^{\text{tem}} = \mathcal{Q}_{\ell_t} \cup \{(f_t, h_t)\}$.

The feature diversity score \mathcal{S}_{div} is defined via multi-scale geometric analysis, capturing both local and global distributional properties, where "local" refers to neighborhood sensitivity (γ), and "global" denotes angular diversity relative to the cache:

$$\mathcal{S}_{\text{div}}(f_k) = \frac{1}{|\mathcal{Q}_{\ell_t}^{\text{tem}}|} \sum_{j \in \mathcal{Q}_{\ell_t}^{\text{tem}}, j \neq k} \left(1 - \frac{f_k \cdot f_j}{\|f_k\|_2 \|f_j\|_2} \right) \cdot \exp(-\gamma \|f_k - f_j\|_2^2), \quad (3)$$

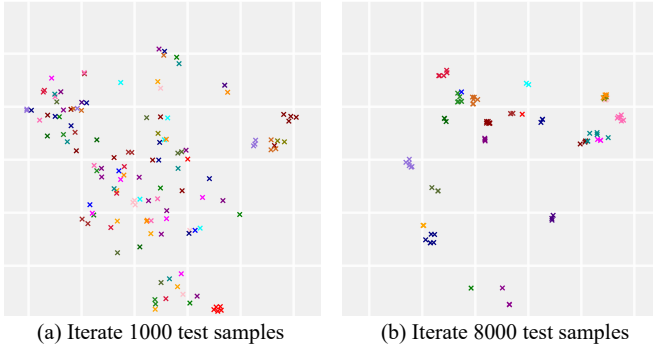


Fig. 4. t-SNE visualizations of priority queue image features. As more samples are incorporated, features from each class form progressively tighter clusters, demonstrating improved representativeness.

where $\gamma > 0$ is a bandwidth parameter controlling locality sensitivity. This formulation combines cosine dissimilarity (capturing angular differences) and Gaussian-weighted Euclidean distance (capturing magnitude differences) to assess diversity.

The confidence score $\mathcal{S}_{\text{conf}}$ transforms prediction logits into a certainty measure using normalized entropy:

$$\begin{aligned} \mathcal{S}_{\text{conf}}(h_k) &= 1 - \frac{\mathcal{H}(h_k)}{\max_{j \in \mathcal{Q}_{\ell_t}^{\text{em}}} \mathcal{H}(h_j)} \\ &= 1 - \frac{-\sum_{c=1}^C h_k^{(c)} \log h_k^{(c)}}{\max_{j \in \mathcal{Q}_{\ell_t}^{\text{em}}} \mathcal{H}(h_j)}, \end{aligned} \quad (4)$$

where $\mathcal{H}(h_k)$ is the entropy of the prediction distribution. Higher confidence (lower entropy) yields higher $\mathcal{S}_{\text{conf}}$.

The joint selection score balances diversity and confidence via adaptive weighting:

$$\mathcal{S}_{\text{joint}}(f_k, h_k) = \tau \cdot \mathcal{S}_{\text{div}}(f_k) + (1 - \tau) \cdot \mathcal{S}_{\text{conf}}(h_k), \quad (5)$$

where $\tau \in [0, 1]$ adjusts the trade-off between diversity and confidence. By ranking $\mathcal{Q}_{\ell_t}^{\text{em}}$ using $\mathcal{S}_{\text{joint}}$ and retaining the top- K samples, we ensure the cache contains high-confidence samples with distinct inter-class separability and diverse intra-class distributions, improving cache hit rates and retrieval effectiveness.

Fig. 4 presents t-SNE [46] visualizations of features stored in \mathcal{Q}_c ($K = 6$) on HICO-DET after 1000 (left) and 8000 (right) updates. Highlighting 25 random classes, the plots demonstrate progressive refinement of CJCS representativeness: features form tighter clusters over time, with semantically similar interactions clustering coherently, validating the cache’s ability to capture discriminative HOI patterns. Note that verb-sharing interactions (with distinct objects) naturally co-cluster due to shared verb semantics, which does not impair performance as object priors resolve ambiguities during inference.

B. Frequency-Aware Cache Adaptation

To further mitigate uncertainty in predicting rare samples, we propose a Frequency-Aware Cache Adaptation (FACA)

strategy that dynamically allocates and populates cache capacity based on class-specific statistical properties. Unlike conventional fixed-capacity approaches, FACA formulates cache management as an optimization objective that balances representational adequacy for rare classes and computational efficiency, ensuring appropriate resource allocation across the long-tail distribution.

Given a frequency distribution $\mathcal{N} = [n_1, n_2, \dots, n_C]$ (where n_c denotes the occurrence count of class c), the adaptive capacity function is defined as:

$$K_c(\mathcal{N}) = K_{\text{base}} \cdot \mathcal{G}(n_c), \quad (6)$$

where $\mathcal{G}(n_c)$ is a parametric scaling function designed for inverse frequency-based allocation:

$$\mathcal{G}(n_c) = \left(\frac{n_{\text{max}} + \gamma}{n_c + \gamma} \right)^\alpha \cdot \exp \left(-\lambda \cdot \frac{n_c}{n_{\text{total}}} \right). \quad (7)$$

The left term establishes an inverse frequency relationship: classes with lower occurrence frequencies receive larger capacity allocations. The smoothing parameter $\gamma > 0$ avoids numerical instability for zero-frequency classes, and $\alpha \in (0, 1]$ controls allocation intensity. The right term introduces relative frequency modulation with $n_{\text{total}} = \sum_{i=1}^C n_i$. Computed capacities are then bounded as:

$$K_c^{\text{final}} = \text{Clip}(\lfloor K_c(\mathcal{N}) \rfloor, K_{\text{min}}, K_{\text{max}}), \quad (8)$$

where $\lfloor \cdot \rfloor$ ensures integer values, and Clip enforces $K_{\text{min}} \leq K_c^{\text{final}} \leq K_{\text{max}}$.

However, a critical challenge arises: rare classes often cannot fully utilize their allocated capacity due to inherent sample scarcity (*i.e.*, $|\mathcal{Q}_c| < K_c^{\text{final}}$). To maximize the utilization of frequency-aware capacity while preserving distributional integrity, we complete the cache through controlled feature augmentation. For each under-capacity class c , we apply stochastic geometric transformations (random cropping, scaling, shearing and so on) to existing entries in \mathcal{Q}_c . The top- ΔK_c augmented samples $\mathbf{z}_{\text{aug}}^{(i)}$ with the highest joint confidence scores $\mathcal{S}_{\text{joint}}(f_k, h_k)$ are selected:

$$\mathcal{Q}_c^{\text{final}} = \mathcal{Q}_c \cup \text{TopK}_{\mathcal{S}_{\text{joint}}}(\mathbf{z}_{\text{aug}}^{(i)}, \Delta K_c), \quad (9)$$

where $\Delta K_c = K_c^{\text{final}} - |\mathcal{Q}_c|$. This completion mechanism ensures rare classes receive adequate representational capacity without introducing distributional bias.

During inference, given the feature $f_p \in \mathbb{R}^d$ of an HOI pair and object category o_{pred} , we retrieve cached entries $\mathcal{S}_o = \{(f_i, h_i)\} \subset \mathcal{Q}_c^{\text{final}}$ and construct key-value matrices:

$$\mathbf{K} = [f_1; f_2; \dots; f_{|\mathcal{S}_o|}] \in \mathbb{R}^{|\mathcal{S}_o| \times d}, \quad (10)$$

$$\mathbf{V} = \text{Onehot}([h_1, h_2, \dots, h_{|\mathcal{S}_o|}]) \in \mathbb{R}^{|\mathcal{S}_o| \times N_c}. \quad (11)$$

The cache logits are computed through affinity-weighted retrieval. The affinity vector is computed via dot product:

$$\mathbf{a} = f_p \mathbf{K}^\top \in \mathbb{R}^{|\mathcal{S}_o|}. \quad (12)$$

The cache logits are then obtained through exponential weighting:

$$\mathbf{w} = \exp(\beta(\mathbf{a} - \mathbf{1})) \in \mathbb{R}^{|\mathcal{S}_o|}, \quad (13)$$

$$\mathbf{logit}_{\text{cache}} = \alpha \cdot \mathbf{w}^\top \mathbf{V} \in \mathbb{R}^{N_c}, \quad (14)$$

where $\mathbf{1}$ is the all-ones vector, α controls cache contribution and β modulates affinity sensitivity. The final prediction combines base detector output with cache-based logits:

$$\mathbf{logit}_{\text{final}} = \mathbf{logit}_{\text{base}} + \mathbf{logit}_{\text{cache}}. \quad (15)$$

IV. EXPERIMENTS

A. Datasets and Metrics

1) *Datasets*: We conduct experiments on two widely-used HOI detection datasets, HICO-DET [47] and V-COCO [48]. The HICO-DET dataset is a large-scale benchmark for HOI detection. It defines 600 interaction types as combinations of 80 object categories and 117 action classes. The dataset comprises 38,118 training images and 9,658 test images, supporting comprehensive model training and evaluation. In contrast to HICO-DET, the V-COCO dataset is much smaller in scale, containing 5,400 train-val images and 4,946 test images. It includes 80 object categories, 29 action classes, and 263 interaction types. V-COCO offers complementary evaluation scenarios with distinct interaction complexities and distribution characteristics.

2) *Metrics*: We adopt the mean Average Precision (mAP) as the primary evaluation metric, following [47]. For HICO-DET, we report mAP scores with three different category configurations: (1) *Full*: evaluation on all 600 interaction types; (2) *Rare*: evaluation on long-tail categories with fewer than 10 training samples; (3) *Non-rare*: evaluation on the remaining categories with sufficient training data. For V-COCO, we report the role mAP under the Scene 1 setting, which evaluates performance across all interaction types following the standard evaluation protocol.

B. Implementation Details

We employ DETR [49] as the object detector, which has been pre-trained on HICO-DET and V-COCO datasets with a ResNet-50 backbone. We adopt ADA-CM [50] as the baseline model and freeze all network parameters. In test-time adaptation, we first feed the entire test set into the model to obtain a complete cache initialization, and subsequently utilize the established cache to generate final prediction results while continuing to update the cache using the enhanced predictions. In the FACA module, we apply random feature augmentation operations, including crop, rotate, shear, and translate, to both human and object features, generating 64 augmented features for each sample and selecting the top 10% with the lowest self-entropy values. The augmentation intensity is controlled by a severity parameter, which is set to 1 by default, and the shot capacity K of the cache is configured to 6. All experiments are conducted with a single Tesla A100 40GB GPU. It is worth noting that ADC can be seamlessly integrated into different architectural paradigms without modification, as demonstrated by our experiments across multiple baseline models. The only requirement is that the base detector outputs interaction logits during inference, making it applicable to virtually all existing HOI methods.

TABLE I
PERFORMANCE COMPARISON ON HICO-DET AND V-COCO DATASETS.
OUR ADC MODULE CONSISTENTLY IMPROVES BASELINE METHODS
ACROSS ALL METRICS.

Method	Backbone	HICO-DET			V-COCO
		Full	Rare	Non-rare	$AP_{\text{role}}^{\#1}$
iCAN [1]	R50	14.84	10.45	16.15	45.3
DRG [51]	R50-F	24.53	19.47	26.04	51.0
HOTR [52]	R50	25.10	17.34	27.42	55.2
QPIC [53]	R50	29.07	21.85	31.23	58.8
CPC [54]	R50	29.63	23.14	31.57	63.1
FGAHOI [55]	Swin-T	29.94	22.24	32.24	60.5
RLIP [56]	R50	32.84	26.85	34.63	61.9
UPT [57]	R50	32.62	28.62	33.81	59.0
GENVLKT [24]	R50	33.75	29.25	35.10	62.4
PViC [58]	R50	34.69	32.14	35.45	62.8
HOICLIP [25]	R50	34.69	31.12	35.74	63.5
RLIPv2 [59]	R50	35.38	29.61	37.10	65.9
LOGICHOI [60]	R50	35.47	32.03	36.22	64.4
ViPLO [61]	ViT-B	37.22	35.45	37.75	62.2
SCTC [62]	R50	37.92	34.78	38.86	67.1
<hr/>					
HOIGEN [8]	R50	33.56	32.10	34.00	-
+ BoostAdapter [45]	R50	34.83	35.37	34.47	-
+ ADC	R50	37.95	40.67	37.14	-
Δ	-	+4.39	+8.57	+3.14	-
<hr/>					
EZ-HOI [9]	R50	38.33	36.70	38.82	60.5
+ BoostAdapter [45]	R50	35.45	34.58	38.35	61.3
+ ADC	R50	39.80	41.85	39.20	64.5
Δ	-	+1.47	+5.15	+0.38	+4.0
<hr/>					
ADA-CM [50]	R50	38.39	37.46	38.67	58.5
+ BoostAdapter [45]	R50	38.75	39.01	38.68	59.9
+ ADC	R50	39.81	41.48	39.30	62.9
Δ	-	+1.41	+3.96	+0.64	+4.4

C. Comparison with State-of-the-Art

Tab. I presents performance comparisons of our ADC module integrated with different baseline methods on HICO-DET and V-COCO datasets. When equipped with the ADC module, ADA-CM with a ResNet-50 backbone achieves 39.81 full mAP and an impressive 41.48 mAP on the rare split, establishing new state-of-the-art performance. Compared to BoostAdapter, a representative TTA method, ADC demonstrates superior performance gains: while BoostAdapter achieves modest improvements (**+0.36 mAP full**, **+1.55 mAP rare** for ADA-CM), our method delivers substantially larger gains (**+1.41 mAP full**, **+3.96 mAP rare**). This indicates that our approach successfully addresses the fundamental challenge of long-tail distribution without sacrificing performance on non-rare categories. Furthermore, the plug-and-play nature of our ADC module is validated by its consistent effectiveness across different baseline methods. As shown in Tab. I, ADC achieves improvements when integrated with HOIGEN (**+8.57 mAP** on rare categories) and EZ-HOI (**+5.15 mAP** on rare categories), demonstrating its broad applicability and generalization capability.

On V-COCO, ADC achieves 62.9 $AP_{\text{role}}^{\#1}$, which represents a notable improvement over our backbone model ADA-CM (58.5 $AP_{\text{role}}^{\#1}$, **+4.4 mAP**) but falls slightly short of the best method SCTC. This performance can be attributed to the

TABLE II
ABLATION STUDY ON HICO-DET DATASET. EACH ADDITIONAL COMPONENT BRINGS CONSISTENT IMPROVEMENTS.

CJCS		FACA		Full	Rare	Non-rare
S_{conf}	S_{div}	K_c^{final}	z_{aug}			
✓				38.39	37.46	38.67
✓	✓			38.79	39.63	38.54
✓	✓	✓		39.47	40.32	39.21
✓	✓	✓	✓	39.81	41.48	39.30

characteristics of the V-COCO dataset: with only 29 actions and 263 interaction types, V-COCO exhibits a more balanced class distribution with less pronounced long-tail effects. Since our method is specifically designed to address long-tail bias through ADC, the more balanced distribution in V-COCO naturally presents a different evaluation scenario compared to highly imbalanced datasets. Nevertheless, the improvement over the baseline model demonstrates the general applicability of our approach, and the more substantial gains on HICO-DET highlight its strength in addressing severe distribution imbalance, which aligns with the core motivation of our design.

D. Ablation Studies

1) *Ablation Study of ADC Components:* To systematically validate the effectiveness of the proposed components and analyze their individual contributions, we conduct ablation experiments on each module. As shown in Tab. II, starting from a baseline configuration (ADA-CM), we progressively add components and evaluate results across all metrics. From the experimental results, it can be observed that each additional component brings consistent improvements, with the complete method achieving optimal performance across all metrics. This effectiveness stems from addressing the fundamental issue of insufficient representative samples for rare interactions during training: CJCS expands the reference pool beyond the limited training set by caching high-quality diverse examples; K_c^{final} in FACA concentrates cache capacity where maximum impact is achieved while reasonably constraining the cache capacity range, and z_{aug} provides additional gains through enhanced knowledge transfer. Each component complements the others, with their combination yielding the highest performance across all metrics.

2) *Discussion of Cache Capacity in ACA:* To investigate the impact of cache capacity on ACA implementation, we conduct experiments evaluating different cache capacities, as shown in Fig. 5. The experimental results demonstrate that cache capacity significantly impacts model performance. Cache capacity of 6 achieves optimal results, while both lower and higher capacities yield suboptimal performance. Notably, rare categories exhibit more substantial improvements from increased capacity (+1.16% from capacity 3 to 6), compared to modest improvements in non-rare categories (+0.09%).

To further understand the underlying mechanisms behind this non-monotonic relationship between capacity and performance, we analyze the evolution of average cache quality

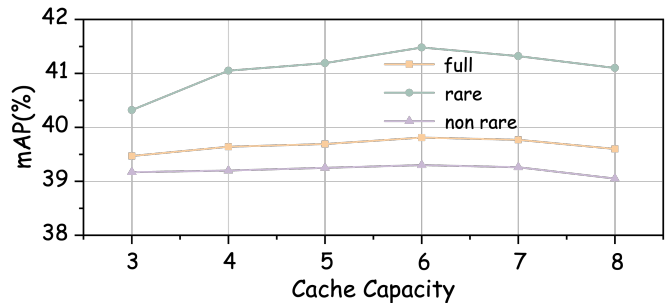


Fig. 5. Effect of cache capacity on model performance. Cache capacity of 6 achieves optimal performance balance across all metrics.

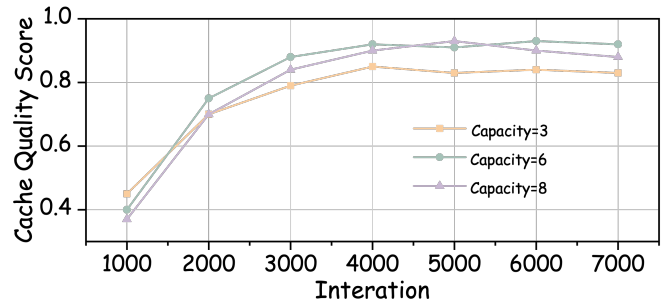


Fig. 6. Comparative analysis of cache quality (average S_{joint}) across different capacities. Cache capacity of 6 achieves the highest peak score (0.93) and maintains stability throughout inference.

across different capacities during inference iterations. We use the CJCS criterion, as presented in Fig. 6. The quality analysis reveals three distinct patterns. Lower capacities experience quality saturation with limited upper bounds. Higher capacities suffer from quality fluctuations and degradation in later iterations. In contrast, moderate capacities maintain stable quality throughout the inference process.

The experimental findings provide key insights into the optimal cache capacity selection. Lower capacities suffer from insufficient historical information storage. This limits the diversity of interaction patterns and contextual references available for prediction, and particularly constrains the detection of underrepresented classes. Conversely, excessively high capacities risk over-dependence on historical judgments and enable storage of low-quality samples that interfere with decision-making. This results in quality degradation and instability caused by conflicting historical information. The moderate capacity strikes an optimal balance between sample quality and information coherence, validating that cache mechanisms primarily enhance rare category detection through improved contextual support while maintaining decision stability across inference iterations.

Furthermore, this stability in cache quality (Fig. 6) demonstrates the model’s inherent robustness to noisy pseudo-labels. As the average joint score progressively increases and stabilizes, the selection mechanism effectively filters out low-confidence entries. Simultaneously, as shown in the t-SNE visualization (Fig. 4), incorrect pseudo-labels typically appear as feature outliers in the latent space. These sparse outliers are statistically suppressed by the dominant signal from the dense,

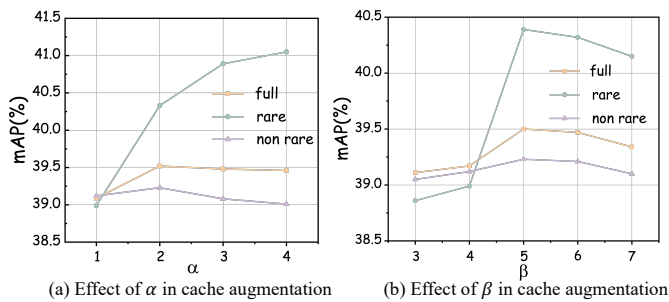


Fig. 7. Effect of α and β in final logits computation on model performance. The scaling factor α demonstrates a clear trade-off between rare and non-rare category performance. The temperature parameter β controls the sharpness of attention distribution over cache entries. Optimal performance is achieved at $\beta = 5$.

correct clusters during the affinity-based retrieval, ensuring that the final predictions remain robust even in the presence of initial noise.

3) *Hyperparameter Sensitivity Analysis*: To understand the sensitivity of hyperparameters in the final logits computation, we conduct ablation studies on the scaling factor α and temperature parameter β , as presented in Fig. 7. The experimental results reveal that the scaling factor α demonstrates a clear trade-off between rare and non-rare category performance, with the highest full mAP achieved at $\alpha = 3$. The temperature parameter β controls the sharpness of the attention distribution over cache entries, with optimal performance achieved at $\beta = 5$.

These observations highlight critical considerations for logits computation. The trade-off observed with α indicates that excessive cache influence can overwhelm the model’s ability to process well-represented categories effectively, while insufficient cache contribution fails to adequately support rare category detection. The temperature parameter β can balance attention distribution: overly uniform attention fails to prioritize relevant cache entries, while excessively sharp focus may lead to over-reliance on limited historical information.

A critical concern for practical deployment is whether these hyperparameters require dataset-specific tuning. Our experiments confirm the robustness of ADC: All main results reported in Tab. I (across different backbones and datasets) use the identical hyperparameter setting ($\alpha = 3, \beta = 5, K = 6$). This demonstrates that ADC does not require careful per-dataset tuning to achieve state-of-the-art performance. As shown in Fig. 7, although optimal values exist, ADC maintains consistent performance gains over the baseline across a wide range of parameter values. The performance does not collapse even with sub-optimal settings, confirming the method’s stability and ease of deployment.

E. Zero-shot Performance Analysis

To evaluate ADC’s effectiveness in zero-shot scenarios, we conduct experiments with different baseline methods on HICO-DET. As shown in Tab. III, in terms of RF-UC and NF-UC settings, our approach marks a significant advancement, particularly for the performance of unseen categories. Relative to the state-of-the-art method EZ-HOI [9], our unseen accuracy

TABLE III
PERFORMANCE COMPARISON ON HICO-DET UNDER UNSEEN COMPOSITION SETTINGS. RF-UC (RARE FIRST) AND NF-UC (NON-RARE FIRST) DENOTE DIFFERENT ZERO-SHOT SPLIT CONFIGURATIONS.

Method	RF-UC Setting			NF-UC Setting		
	Full	Seen	Unseen	Full	Seen	Unseen
GEN-VLKT [24]	30.56	32.91	21.36	23.71	23.38	25.05
HOICLIP [25]	32.99	34.85	25.53	27.75	28.10	26.39
CLIP4HOI [26]	34.08	35.48	28.47	28.90	28.26	31.44
LOGICHOI [60]	33.17	34.93	25.97	27.95	27.86	26.84
ADA-CM [50]	33.01	34.35	27.63	31.39	31.13	32.41
+ ADC (Ours)	38.17	38.73	35.96	36.73	37.17	34.95
Δ	+5.16	+4.38	+8.33	+5.34	+6.04	+2.54
HOIGen [8]	33.86	34.57	31.01	33.08	32.86	33.98
+ ADC (Ours)	35.56	35.78	34.67	36.01	36.47	34.19
Δ	+1.70	+1.21	+3.66	+2.93	+3.61	+0.21
EZ-HOI [9]	36.73	37.35	34.24	34.84	34.47	36.33
+ ADC (Ours)	37.16	37.39	37.06	35.64	34.93	37.48
Δ	+0.43	+0.04	+2.82	+0.80	+0.46	+1.15

TABLE IV
PERFORMANCE COMPARISON ON HICO-DET SYSTEMATIC GENERALIZATION (SG) SPLITS. ADC CONSISTENTLY IMPROVES COMPOSITIONAL GENERALIZATION.

Method	Backbone	SG1	SG2	SG3
EZ-HOI [9]	R50	16.57	14.62	15.73
+ ADC	R50	17.64	15.53	16.42
Δ	-	+1.07	+0.91	+0.69
ADA-CM [50]	R50	15.64	15.02	15.76
+ ADC	R50	17.16	16.93	17.01
Δ	-	+1.52	+1.91	+1.25
HOIGEN [8]	R50	14.40	13.27	14.53
+ ADC	R50	16.27	15.66	16.28
Δ	-	+1.87	+2.39	+1.75

achieves a consistent gain of 0.43% and 0.80% for RF-UC and NF-UC, respectively. This is because the baseline model’s zero-shot design enables the cache to accumulate reliable interaction patterns even for rare/unseen categories, which ADC can effectively leverage. Moreover, ADC universally benefits all baseline methods, achieving consistent improvements across the board. Notably, beyond the gains in unseen categories, ADC also simultaneously enhances both Full and Seen mAP, demonstrating its comprehensive effectiveness.

These findings highlight that ADC serves as an amplifier: it enhances the inherent capabilities of the base model, particularly benefiting models with zero-shot design by providing robust historical context for unseen interactions.

F. Systematic Generalization Analysis

To further evaluate the model’s capability in handling the compositional nature of HOI detection—where objects and verbs may appear in novel combinations—we conduct experiments on the HICO-DET-SG (Systematic Generalization) splits [23]. Unlike standard random splits, SG splits are

TABLE V
EFFICIENCY AND PERFORMANCE ANALYSIS IN ONLINE STREAMING SETTING. WE REPORT THE INFERENCE TIME AND MEMORY COST ON THE FULL TEST SET OF HICO-DET AND V-COCO RESPECTIVELY.

Method	HICO-DET (Online)				V-COCO (Online)		
	mAP		Cost		mAP	Cost	
	Full	Rare	Time	Mem.	AP ^{#1}	Time	Mem.
EZ-HOI [9]	38.33	36.70	1h 23m	7619M	60.50	23m	6822M
+ ADC	38.81	39.57	2h 20m	8926M	60.97	39m	8410M
ADA-CM [50]	38.39	37.46	11m	4886M	58.50	8m	4758M
+ ADC	39.48	40.60	39m	6908M	61.90	14m	6916M
HOI-Gen [8]	33.56	32.10	12m	4612M	-	-	-
+ ADC	36.03	39.46	17m	4920M	-	-	-

designed to test the model’s ability to recombine learned concepts for unseen triplets.

As shown in Tab. IV, ADC achieves consistent improvements across all three systematic generalization splits (SG1, SG2, SG3). Specifically, on the challenging SG1 split, ADC boosts the performance of EZ-HOI and ADA-CM by **1.07%** and **1.52%** mAP, respectively. This indicates that while our method focuses on mitigating long-tail bias via frequency-aware caching, the diversity mechanism in ADC effectively retrieves high-quality historical prototypes to “patch” unreliable predictions for rare or unseen compositions. This confirms that ADC not only addresses frequency imbalance but also enhances the model’s compositional generalization capability.

G. Efficiency and Online Adaptation Analysis

1) *Computational Overhead:* We analyze the computational cost of ADC in terms of inference time and memory usage. As presented in Tab. V, compared to the base models, ADC introduces a negligible memory overhead (e.g., increasing from 7619M to 8926M for EZ-HOI), as we only store lightweight feature vectors rather than heavy model parameters. Regarding time efficiency, while the retrieval mechanism introduces additional latency (approximately 1.4×–3.5×), it remains far more efficient than standard gradient-based adaptation methods (which typically require 6–10× latency). This represents a superior trade-off between efficiency and the substantial accuracy gains observed.

2) *Online Setting:* We further evaluate ADC in a realistic Online setting, where the cache is built incrementally from scratch. As shown in Tab. V, we report results on both HICO-DET and V-COCO. Although the “cold start” problem leads to slightly lower performance compared to the Offline setting, ADC still achieves robust improvements over the static baseline (+1.09 mAP), further verifying its effectiveness across different datasets. This confirms that our Confidence-Diversity Joint Cache Selection (CJCS) mechanism can effectively curate high-quality features on-the-fly.

H. Qualitative Results

To demonstrate the effectiveness of our method, we present several qualitative results across two distinct and representative scenarios, as shown in Fig. 8(a). In challenging cases



Fig. 8. Qualitative results comparing HOI detection with and without ADC, based on ADA-CM backbone. The gray bar represents the rare class prediction, and the blue bar represents the non-rare class prediction. (a) Scenarios with rare interactions; (b) Scenarios without rare interactions.

involving rare interactions, ADC successfully corrects the baseline model’s errors by recovering missed rare categories, providing crucial historical context that enables the model to recognize underrepresented interaction patterns that would otherwise remain undetected. For cases where the baseline model can detect all ground-truth interactions (Fig. 8(b)), ADC demonstrates its ability to enhance prediction quality by providing more discriminative confidence scores. Specifically, ADC suppresses the confidence scores of incorrect interaction predictions while boosting the scores of correct ones, thereby creating clearer decision boundaries and reducing false positive detections. This demonstrates that ADC not only enhances recall for rare categories but also improves overall precision by leveraging cached knowledge to provide more reliable confidence calibration, leading to more robust and accurate HOI detection performance across diverse interaction scenarios.

V. CONCLUSION

In this paper, we present ADC module, a novel training-free and plug-and-play solution to address the long-tail distribution challenge in HOI detection. ADC enables dynamic accumulation and adaptive augmentation of diverse feature representations during inference to substantially enhance the recognition of rare interactions without requiring additional training or model modifications. Extensive experiments across multiple HOI benchmarks demonstrate that ADC not only significantly improves performance on underrepresented categories, but also maintains competitive results on frequent interactions. These findings highlight the potential of ADC as a practical and scalable solution for fair and robust HOI detection. Overall, this work opens new avenues for addressing long-tail challenges in HOI detection by leveraging training-free dynamic adaptation mechanisms. In future work, ADC could be extended to other long-tailed structured prediction tasks, such as visual grounding or action segmentation, and integrated into continual learning frameworks to enhance adaptation under evolving data distributions.

REFERENCES

- [1] C. Gao, Y. Zou, and J.-B. Huang, “iCAN: Instance-centric attention network for HOI detection,” *arXiv preprint arXiv:1808.10437*, 2018.
- [2] S. Fang, Z. Lin, K. Yan, J. Li, X. Lin, and R. Ji, “Hodn: Disentangling human-object feature for hoi detection,” *IEEE Transactions on Multimedia*, vol. 26, pp. 3125–3136, 2023.
- [3] D. Chen, D. Kong, J. Gao, J. Li, Q. Li, and B. Yin, “Ask-hoi: Affordance-scene knowledge prompting for human-object interaction detection,” *IEEE Transactions on Multimedia*, vol. 28, pp. 742–756, 2025.
- [4] M. Jia, L. Zhao, G. Li, and Y. Zheng, “ContextHOI: Spatial context learning for HOI detection,” in *Proc. AAAI Conf. Artif. Intell.*, 2025, pp. 3931–3939.
- [5] X. Liu, Y.-L. Li, X. Wu, Y.-W. Tai, C. Lu, and C.-K. Tang, “Interactiveness field in HOI,” in *Proc. IEEE/CVF Conf. Comput. Vis. Pattern Recognit. (CVPR)*, 2022, pp. 20 113–20 122.
- [6] M. Wu, Y. Liu, J. Ji, X. Sun, and R. Ji, “Toward open-set HOI detection,” in *Proc. AAAI Conf. Artif. Intell.*, 2024, pp. 6066–6073.
- [7] J. Gao, K. Liang, T. Wei, W. Chen, Z. Ma, and J. Guo, “Dual-prior augmented decoding network for long tail distribution in HOI detection,” in *Proc. AAAI Conf. Artif. Intell.*, 2024, pp. 1806–1814.
- [8] Y. Guo, Y. Liu, J. Li, W. Wang, and Q. Jia, “Unseen no more: Unlocking the potential of CLIP for generative zero-shot HOI detection,” in *Proc. ACM Int. Conf. Multimedia (MM)*, 2024, pp. 1711–1720.
- [9] Q. Lei, B. Wang, and R. Tan, “EZ-HOI: VLM adaptation via guided prompt learning for zero-shot HOI detection,” in *Proc. Adv. Neural Inf. Process. Syst. (NeurIPS)*, 2024, pp. 55 831–55 857.
- [10] W. Li, R. Zhang, R. Shao, J. He, and L. Nie, “CogVLA: Cognition-aligned vision-language-action model via instruction-driven routing & sparsification,” *arXiv preprint arXiv:2508.21046*, 2025.
- [11] X. Li, P. Sun, Y. Liu, L. Duan, and W. Li, “Simultaneous detection and interaction reasoning for object-centric action recognition,” *IEEE Transactions on Multimedia*, 2025.
- [12] H. Jhuang, J. Gall, S. Zuffi, C. Schmid, and M. J. Black, “Towards understanding action recognition,” in *Proc. IEEE/CVF Int. Conf. Comput. Vis. (ICCV)*, 2013, pp. 3192–3199.
- [13] Z. Sun, Q. Ke, H. Rahmani, M. Bennamoun, G. Wang, and J. Liu, “Human action recognition from various data modalities: A review,” *IEEE Trans. Pattern Anal. Mach. Intell.*, vol. 45, no. 3, pp. 3200–3225, 2022.
- [14] K. Li, D. Guo, G. Chen, C. Fan, J. Xu, Z. Wu, H. Fan, and M. Wang, “Prototypical calibrating ambiguous samples for micro-action recognition,” in *Proc. AAAI Conf. Artif. Intell.*, 2025, pp. 4815–4823.
- [15] B. Li, M. Liu, G. Wang, and Y. Yu, “Frame order matters: A temporal sequence-aware model for few-shot action recognition,” in *Proc. AAAI Conf. Artif. Intell.*, 2025, pp. 18 218–18 226.
- [16] A. Vosoughi, S. Deng, S. Zhang, Y. Tian, C. Xu, and J. Luo, “Cross modality bias in visual question answering: A causal view with possible worlds vqa,” *IEEE Transactions on Multimedia*, vol. 26, pp. 8609–8624, 2024.
- [17] S. Antol, A. Agrawal, J. Lu, M. Mitchell, D. Batra, C. L. Zitnick, and D. Parikh, “VQA: Visual question answering,” in *Proc. IEEE/CVF Int. Conf. Comput. Vis. (ICCV)*, 2015, pp. 2425–2433.
- [18] S. Yang, S. Luo, and S. C. Han, “Multimodal commonsense knowledge distillation for visual question answering (student abstract),” in *Proc. AAAI Conf. Artif. Intell.*, 2025, pp. 29 545–29 547.
- [19] F. Cocchi, N. Moratelli, M. Cornia, L. Baraldi, and R. Cucchiara, “Augmenting multimodal LLMs with self-reflective tokens for knowledge-based visual question answering,” in *Proc. IEEE/CVF Conf. Comput. Vis. Pattern Recognit. (CVPR)*, 2025, pp. 9199–9209.
- [20] W. Li, B. Hu, R. Shao, L. Shen, and L. Nie, “Lion-FS: Fast & slow video-language thinker as online video assistant,” in *Proc. IEEE/CVF Conf. Comput. Vis. Pattern Recognit. (CVPR)*, 2025, pp. 3240–3251.
- [21] A. Radford, J. W. Kim, C. Hallacy, A. Ramesh, G. Goh, S. Agarwal, G. Sastry, A. Askell, P. Mishkin, J. Clark *et al.*, “Learning transferable visual models from natural language supervision,” in *Proc. Int. Conf. Mach. Learn. (ICML)*, 2021, pp. 8748–8763.
- [22] J.-B. Alayrac *et al.*, “Flamingo: A visual language model for few-shot learning,” in *Proc. Adv. Neural Inf. Process. Syst. (NeurIPS)*, 2022, pp. 23 716–23 736.
- [23] Z. Hou, B. Yu, Y. Qiao, X. Peng, and D. Tao, “Detecting HOI via fabricated compositional learning,” in *Proc. IEEE/CVF Conf. Comput. Vis. Pattern Recognit. (CVPR)*, 2021, pp. 14 646–14 655.
- [24] Y. Liao, A. Zhang, M. Lu, Y. Wang, X. Li, and S. Liu, “GEN-VLKT: Simplify association and enhance interaction understanding for HOI detection,” in *Proc. IEEE/CVF Conf. Comput. Vis. Pattern Recognit. (CVPR)*, 2022, pp. 20 123–20 132.
- [25] S. Ning, L. Qiu, Y. Liu, and X. He, “HOICLIP: Efficient knowledge transfer for HOI detection with vision-language models,” in *Proc. IEEE/CVF Conf. Comput. Vis. Pattern Recognit. (CVPR)*, 2023, pp. 23 507–23 517.
- [26] Y. Mao, J. Deng, W. Zhou, L. Li, Y. Fang, and H. Li, “CLIP4HOI: Towards adapting CLIP for practical zero-shot HOI detection,” in *Proc. Adv. Neural Inf. Process. Syst. (NeurIPS)*, 2023, pp. 45 895–45 906.
- [27] Y. Cao, Q. Tang, X. Su, S. Chen, S. You, X. Lu, and C. Xu, “Detecting any HOI relationship: Universal HOI detector with spatial prompt learning on foundation models,” in *Proc. Adv. Neural Inf. Process. Syst. (NeurIPS)*, 2023, pp. 739–751.
- [28] J. Xiao, Z. Sun, H. An, H. Zhao, M. Qiu, and X. Li, “Optical image processing and applications empowered by vision-language models,” *iOptics*, vol. 1, no. 1, p. 100003, 2025.
- [29] Y. Chen, H. An, Z. Sun, T. Tian, M. Chen, C. Spielmann, and X. Li, “Large model enhanced computational ghost imaging,” *Science China Technological Sciences*, vol. 68, no. 11, p. 2120403, 2025.
- [30] Y. Qi, H. Li, Y. Song, X. Wu, and J. Luo, “How vision-language tasks benefit from large pre-trained models: A survey,” *IEEE Transactions on Multimedia*, 2025.
- [31] M. U. Khattak, H. Rasheed, M. Maaz, S. Khan, and F. S. Khan, “MaPLE: Multi-modal prompt learning,” in *Proc. IEEE/CVF Conf. Comput. Vis. Pattern Recognit. (CVPR)*, 2023, pp. 19 113–19 122.
- [32] G. Wang, C. Ding, W. Tan, and M. Tan, “Decoupled prototype learning for reliable test-time adaptation,” *IEEE Transactions on Multimedia*, vol. 27, pp. 3585–3597, 2025.
- [33] D. Wang, E. Shelhamer, S. Liu, B. Olshausen, and T. Darrell, “TENT: Fully test-time adaptation by entropy minimization,” *arXiv preprint arXiv:2006.10726*, 2020.
- [34] X. Qiao, P. Huang, J. Yuan, X. Guo, B. Ye, Z. Sun, and X. Li, “Bidirectional prototype-reward co-evolution for test-time adaptation of vision-language models,” *arXiv preprint arXiv:2503.09394*, 2025.
- [35] Y. Sun, X. Wang, Z. Liu, J. Miller, A. Efros, and M. Hardt, “Test-time training with self-supervision for generalization under distribution shifts,” in *Proc. Int. Conf. Mach. Learn. (ICML)*, 2020, pp. 9229–9248.
- [36] D. Chen, D. Wang, T. Darrell, and S. Ebrahimi, “Contrastive test-time adaptation,” in *Proc. IEEE/CVF Conf. Comput. Vis. Pattern Recognit. (CVPR)*, 2022, pp. 295–305.
- [37] A. Karmanov, D. Guan, S. Lu, A. E. Saddik, and E. Xing, “Efficient test-time adaptation of vision-language models,” in *Proc. IEEE/CVF Conf. Comput. Vis. Pattern Recognit. (CVPR)*, 2024, pp. 14 162–14 171.
- [38] C. Zhang, S. Stepputtis, K. Sycara, and Y. Xie, “Dual prototype evolving for test-time generalization of vision-language models,” in *Proc. Adv. Neural Inf. Process. Syst. (NeurIPS)*, 2024, pp. 32 111–32 136.
- [39] M. Hu, T. Song, Y. Gu, X. Luo, J. Chen, Y. Chen, Y. Zhang, and S. Zhang, “Fully test-time adaptation for image segmentation,” in *Proc. Int. Conf. Med. Image Comput. Comput.-Assist. Intervent.*, 2021, pp. 251–260.
- [40] I. Shin, Y.-H. Tsai, B. Zhuang, S. Schuster, B. Liu, S. Garg, I. S. Kweon, and K.-J. Yoon, “MM-TTA: Multi-modal test-time adaptation for 3D semantic segmentation,” in *Proc. IEEE/CVF Conf. Comput. Vis. Pattern Recognit. (CVPR)*, 2022, pp. 16 928–16 937.
- [41] Z. Deng, Z. Chen, S. Niu, T. Li, B. Zhuang, and M. Tan, “Efficient test-time adaptation for super-resolution with second-order degradation and reconstruction,” in *Proc. Adv. Neural Inf. Process. Syst. (NeurIPS)*, 2023, pp. 74 671–74 701.
- [42] A. Shocher, N. Cohen, and M. Irani, ““Zero-shot” super-resolution using deep internal learning,” in *Proc. IEEE/CVF Conf. Comput. Vis. Pattern Recognit. (CVPR)*, 2018, pp. 3118–3126.
- [43] X. Ruan and W. Tang, “Fully test-time adaptation for object detection,” in *Proc. IEEE/CVF Conf. Comput. Vis. Pattern Recognit. (CVPR)*, 2024, pp. 1038–1047.
- [44] O. Veksler, “Test time adaptation with regularized loss for weakly supervised salient object detection,” in *Proc. IEEE/CVF Conf. Comput. Vis. Pattern Recognit. (CVPR)*, 2023, pp. 7360–7369.
- [45] T. Zhang, J. Wang, H. Guo, T. Dai, B. Chen, and S.-T. Xia, “Boost-Adapter: Improving vision-language test-time adaptation via regional bootstrapping,” in *Proc. Adv. Neural Inf. Process. Syst. (NeurIPS)*, 2024, pp. 67 795–67 825.
- [46] G. Hinton and L. V. D. Maaten, “Visualizing data using t-SNE,” *J. Mach. Learn. Res.*, vol. 9, pp. 2579–2605, 2008.
- [47] Y.-W. Chao, Y. Liu, X. Liu, H. Zeng, and J. Deng, “Learning to detect HOI,” in *Proc. IEEE Winter Conf. Appl. Comput. Vis. (WACV)*, 2018, pp. 381–389.
- [48] S. Gupta and J. Malik, “Visual semantic role labeling,” *arXiv preprint arXiv:1505.04474*, 2015.

- [49] N. Carion, F. Massa, G. Synnaeve, N. Usunier, A. Kirillov, and S. Zagoruyko, "End-to-end object detection with transformers," in *Proc. Eur. Conf. Comput. Vis. (ECCV)*, 2020, pp. 213–229.
- [50] T. Lei, F. Caba, Q. Chen, H. Jin, Y. Peng, and Y. Liu, "Efficient adaptive HOI detection with concept-guided memory," in *Proc. IEEE/CVF Int. Conf. Comput. Vis. (ICCV)*, 2023, pp. 6480–6490.
- [51] C. Gao, J. Xu, Y. Zou, and J.-B. Huang, "DRG: Dual relation graph for HOI detection," in *Proc. Eur. Conf. Comput. Vis. (ECCV)*, 2020, pp. 696–712.
- [52] B. Kim, J. Lee, J. Kang, E.-S. Kim, and H. J. Kim, "HOTR: End-to-end HOI detection with transformers," in *Proc. IEEE/CVF Conf. Comput. Vis. Pattern Recognit. (CVPR)*, 2021, pp. 74–83.
- [53] M. Tamura, H. Ohashi, and T. Yoshinaga, "QPIC: Query-based pairwise HOI detection with image-wide contextual information," in *Proc. IEEE/CVF Conf. Comput. Vis. Pattern Recognit. (CVPR)*, 2021, pp. 10410–10419.
- [54] J. Park, S. Lee, H. Heo, H. K. Choi, and H. J. Kim, "Consistency learning via decoding path augmentation for transformers in HOI detection," in *Proc. IEEE/CVF Conf. Comput. Vis. Pattern Recognit. (CVPR)*, 2022, pp. 1019–1028.
- [55] S. Ma, Y. Wang, S. Wang, and Y. Wei, "FGAHOI: Fine-grained anchors for HOI detection," *IEEE Trans. Pattern Anal. Mach. Intell.*, vol. 46, no. 4, pp. 2415–2429, 2023.
- [56] H. Yuan, J. Jiang, S. Albanie, T. Feng, Z. Huang, D. Ni, and M. Tang, "RLIP: Relational language-image pre-training for HOI detection," in *Proc. Adv. Neural Inf. Process. Syst. (NeurIPS)*, 2022, pp. 37416–37431.
- [57] F. Z. Zhang, D. Campbell, and S. Gould, "Efficient two-stage detection of HOI with a novel unary-pairwise transformer," in *Proc. IEEE/CVF Conf. Comput. Vis. Pattern Recognit. (CVPR)*, 2022, pp. 20104–20112.
- [58] F. Z. Zhang, Y. Yuan, D. Campbell, Z. Zhong, and S. Gould, "Exploring predicate visual context in detecting of HOI," in *Proc. IEEE/CVF Int. Conf. Comput. Vis. (ICCV)*, 2023, pp. 10411–10421.
- [59] H. Yuan, S. Zhang, X. Wang, S. Albanie, Y. Pan, T. Feng, J. Jiang, D. Ni, Y. Zhang, and D. Zhao, "RLIPv2: Fast scaling of relational language-image pre-training," in *Proc. IEEE/CVF Int. Conf. Comput. Vis. (ICCV)*, 2023, pp. 21649–21661.
- [60] L. Li, J. Wei, W. Wang, and Y. Yang, "Neural-logic HOI detection," in *Proc. Adv. Neural Inf. Process. Syst. (NeurIPS)*, 2023, pp. 21158–21171.
- [61] J. Park, J.-W. Park, and J.-S. Lee, "ViPLO: Vision transformer based pose-conditioned self-loop graph for HOI detection," in *Proc. IEEE/CVF Conf. Comput. Vis. Pattern Recognit. (CVPR)*, 2023, pp. 17152–17162.
- [62] W. Jiang, W. Ren, J. Tian, L. Qu, Z. Wang, and H. Liu, "Exploring self- and cross-triplet correlations for HOI detection," in *Proc. AAAI Conf. Artif. Intell.*, 2024, pp. 2543–2551.